Ann. Geophys. Discuss., https://doi.org/10.5194/angeo-2019-40
Manuscript under review for journal Ann. Geophys.
Discussion started: 26 March 2019

Annales Geophysicae Discussions
Open Access
EGU

Swarm field-aligned currents during a severe magnetic storm of September 2017

Renata Lukianova[1,2]

[1] Space Research Institute, 117997 Moscow, Russia
[2] Institute of Earth Science, Saint Petersburg State University, 199034 Saint Petersburg, Russia

Correspondence to: Renata Lukianova (renata@aari.nw.ru)

Abstract. *Swarm* satellites observations are used to characterize the extreme behavior of large- and small-scale field-aligned currents (FACs) during the severe magnetic storm of September 2017. Evolution of the current intensities and the equatorward displacement of FACs are analyzed while the satellites cross the pre-midnight, pre-noon, dusk and dawn sectors in both hemispheres. The equatorward boundaries of FACs mainly follow the dynamics of ring current (as monitored in terms of the SYM-H index). The minimum latitude of the FAC boundaries is limited to 50° MLat, below which saturation occurs. The FAC densities are very variable and may increase dramatically, especially in the nightside ionosphere during the storm-time substorms. At the peak of substorm, the average FAC densities reach >3 $\mu A/m^2$. The dawn–dusk asymmetry is manifested in the enhanced dusk-side R2 FACs in both hemispheres. Filamentary high-density structures are always observed confirming that a substantial fraction of R1/R2 FACs is composed of many small-scale currents. In the pre-noon sector, the bipolar structures (7.5 km width FACs of opposite polarities adjacent to each other) dominate, while in the post-midnight sector the upward and downward FACs tend to form more latitudinally extended structures of a certain polarity. The most intense small-scale FACs (up to ~80 $\mu A/m^2$) is observed just in the post-midnight sector. Simultaneous magnetic and plasma perturbations indicate that this structure is likely a current system of a mesoscale auroral arc.

Keywords: Ionosphere-magntosphere interaction, Field-alighned currents, Storms and substorms, Auroral arcs electrodynamics

1 Introduction

Field-aligned currents (FACs) provide electrodynamic coupling of the solar wind-magnetosphere-ionosphere system. FACs flow along the high-conducting geomagnetic field lines between the magnetospheric boundary layers and the auroral ionosphere. If a substorm occurs, additional FACs form a current wedge connecting the magnetotail and ionospheric electrojet. During a storm main phase the lower latitude FACs are partly connected to the ring current (Akasofu, 1964; Lui 1996). Schematic distribution of large-scale FACs has been established by Iijima and Potemra (1976). The ionospheric projection of the 3D FAC system consists of a pair of sheets elongated along the auroral oval, namely, Region 1 (R1) and Region 2 (R2), with opposite current flow directions in the morning and evening local time sectors and additional current sheets (R0) located on the dayside poleward of R1/R2. Subsequent space missions allowed constructing comprehensive empirical models of FAC parameterized by the interplanetary magnetic field (IMF) direction and strength, by season, and by hemisphere (Weimer, 2001; Papitashvili et al., 2002; Green at al.,

Ann. Geophys. Discuss., https://doi.org/10.5194/angeo-2019-40
Manuscript under review for journal Ann. Geophys.
Discussion started: 26 March 2019

Annales Geophysicae Discussions

2009). Under stationary conditions the FAC system is evolved in accordance with the dayside reconnection, which is controlled by the solar wind (SW). During a magnetic storm, FACs become highly dynamic because of the release of energy stored previously in the magnetotail and the ring current build up. The FAC intensity increases and may considerably exceed its nominal level. The equatorward expansion, the latitudinal widening and the dawn–dusk asymmetry of the R1/R2 current sheets are also observed (Iijima and Potemra 1978; Wang et al., 2006; Anderson and Korth, 2008). While average current densities typically are of units of $\mu A/m^2$ or less, instantaneous small-scale FACs may reach several hundred $\mu A/m^2$ (Neubert and Christiansen, 2003).

Magnetic storms are characterized by a dramatic enhancement of energy deposition to the Earth's atmosphere. Storm-time FACs are stronger and more variable compared to stationary FACs predicted by the models. Since the intensity and time evolution of FACs vary from storm to storm, it is of interest to analyze their unique characteristics. Utilizing the magnetic field measurements by *CHAMP* satellite Wang et al. (2006) investigated the northern and southern hemisphere dayside and nightside FAC characteristics during the extreme October and November 2003 magnetic storms. Using the global maps from the *Iridium* constellation Anderson and Korth (2008) studied the FACs during severe magnetic storms which occurred during the solar cycle 23 with a particular attention to the evolution of FACs in the course of the storm of August 2000. Since 2014, comprehensive studies of FAC distributions were carried out based on high precision observations onboard of *Swarm* constellation (Dunlop et al., 2015; Juusola et al., 2016; McGranaghan et al., 2017). However, the *Swarm* data have not yet been fully utilized for the storm-time FAC analysis. In this paper we analyze the *Swarm* observations in order to identify various characteristics of the storm-time FACs for the event of 6–9 September 2017, which was one of the two most severe magnetic storms of the recent solar cycle 24 (the previous event was the St-Patrick storm on 17 March 2015). The September 2017 event was a two-step storm during which two intense substorms occurred. The satellites measured FACs with a 1-second cadence in the pre-midnight, pre-noon, dusk and dawn sectors.

2 Space weather conditions on 6–9 September 2017

At the declining phase of solar cycle 24, starting from 6 September 2017, strong multiple solar flares occurred. The associated interplanetary coronal mass ejections collided with Earth's magnetosphere and caused the most intense magnetic storm of the recent solar cycle. The storm produced strong geomagnetic disturbances, ionospheric effects, magnificent auroral displays, elevated hazards to power systems and unstable HF radio wave propagation (Chertok et al., 2018; Clilverd et al., 2018; Curto et al., 2018; Yasyukevich et al., 2018).

Evolution of the SW parameters and geomagnetic activity is presented in **Fig. 1** showing (from top to bottom): the IMF Bz and By, the solar wind proton speed (Vsw) and density (Nsw), the auroral AL and the equatorial SYM-H

Ann. Geophys. Discuss., https://doi.org/10.5194/angeo-2019-40
Manuscript under review for journal Ann. Geophys.
Discussion started: 26 March 2019

Annales Geophysicae Discussions
Open Access
EGU

geomagnetic indices from the OMNI-web service (https://omniweb.gsfc.nasa.gov/). Two SW shock events impact the magnetosphere. The arrival of the first shock late on 6 September results in a sudden increase in all parameters except the AL index. Since IMF Bz turns northward, this initial disturbance is only weakly geoeffective as a result. At 18:30 UT on 7 September, IMF Bz turns southward that triggers a substorm and a ring current build up. The second shock arrived at ~23:30 UT on 7 September, with the SW speed up to 800 km/s and strongly negative Bz and By. This shock causes an abrupt drop of SYM-H down to -150 nT and a spike-like decrease of AL down to -2200 nT. After 01:00, IMF Bz becomes positive, AL gradually approaches to zero and SYM-H is recovered. At ~12 UT on 8 September another strongly negative Bz period is seen, and the SW speed remains high (>700 km/s). This causes the second substorm (AL is -2000 nT) and ring current intensification (SYM-H is -100 nT). A steady recovery occurs in geomagnetic indices throughout 9 September. The SW parameters are not available for this day.

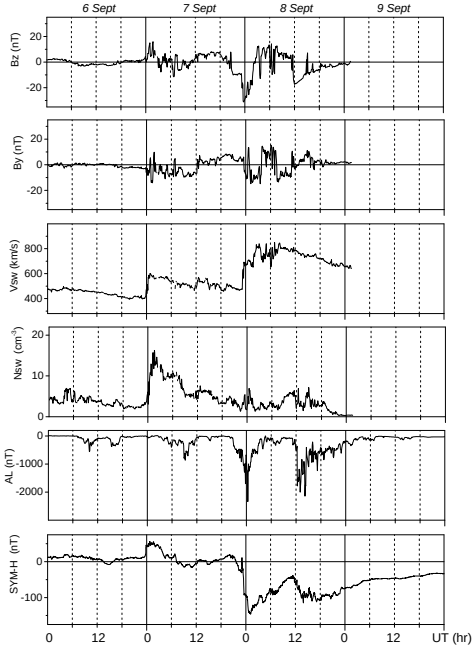

Figure 1: From top to bottom: IMF Bz and By, SW speed and density, AL and SYM-H indices on 6-9 September 2017 (5-min values).

Ann. Geophys. Discuss., https://doi.org/10.5194/angeo-2019-40
Manuscript under review for journal Ann. Geophys.
Discussion started: 26 March 2019

Annales Geophysicae Discussions
Open Access
EGU

3 *Swarm* satellites

The ESA *Swarm* mission is a constellation consisting of the three identical satellites (hereafter SwA, SwB and SwC, respectively), all are at the low-altitude polar orbit. The *Swarm* constellation was launched in the end of 2013 at the orbit altitude of ~465 km (SwA and SwC) and ~520 km (SwB); the orbit inclination is 87.5°. By September 2017 the orbit altitude decreases down to ~440 and 505 km, respectively. SwA and SwC fly in a tandem separated by 1-1.4° in longitude. SwB is separated by about 1.5 hr in local time from the tandem satellites. Slowly drifting in longitude, the orbits cover all the local time sectors over 7-10 months. The main module of the *Swarm* payload is the high-sensitivity vector and scalar magnetometers. From the measured magnetic field variations, which results from FACs, the current densities are computed with a techniques invoking Ampere's law (Ritter and Lühr, 2006). The 1-sec values of FAC densities are available via the on-line *Swarm* data portal (ftp://swarm-diss.eo.esa.int) as Level 2 data products (Swarm Level 2 Processing System Consortium, 2012).

Orbits of the constellation as of September 6-9, 2017 are shown in **Fig. 2**.The polar projection of the satellite orbits in the northern hemisphere is shown in **Fig. 2a**. The successive trajectories (14-15 trajectories per day) are almost parallel to each other and slightly shifted in local time. The satellite SwA (orbits of SwC are very similar) enters the region of MLat>60° at magnetic local times (MLT) between ~09 and 12 MLT, and leave this region between ~21 and 23 MLT. The entry (exit) points of the SwB orbit are located between ~15 and 17 (02 and 04) MLTs. In the southern hemisphere the direction of the tracks in the MLT-MLat framework is opposite. During a day the orbits are rotated systematically but, except the near-pole region (MLat>80°), they stay within the early morning, pre-noon, pre-dawn and pre-midnight sectors. The daily variation of MLTs at which the satellites cross the latitude MLat=60° are shown in **Fig. 2b**. The MLT ranges covered by the tracks are presented in **Table 1**.

Ann. Geophys. Discuss., https://doi.org/10.5194/angeo-2019-40
Manuscript under review for journal Ann. Geophys.
Discussion started: 26 March 2019

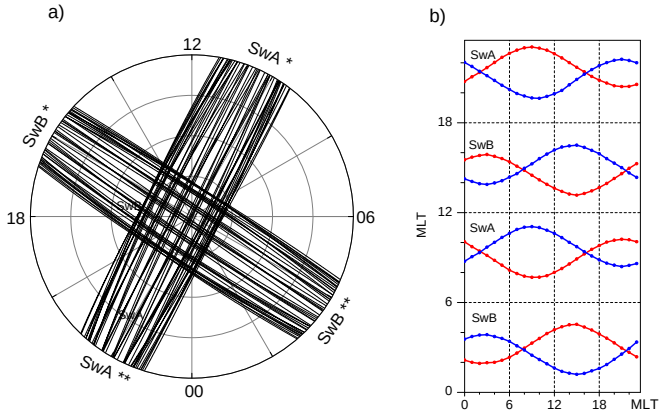

Figure 2: (a) Orbits of SwA and SwB in the northern hemispheres on 6-9 September 2017 in the MLT-Mlat framework. Circles are drawn every 10° down to 50° Mlat. Symbol * and ** indicates the entry and exit point, respectively. **(b)** Daily variation of MLTs at which SwA and SwB cross the latitude MLat=60° in the northern (blue) and southern (red) hemispheres.

Table 1. Parameters of the tracks in the northern and southern polar regions

Satellite	MLT ranges of entry and exit points at 60° MLat (hh:mm)	Center of the MLT range (hh:mm)	Track identifier*
Northern hemisphere			
SwB	02:50-04:40	03:40	N04
SwA (SwC)	09:40-11:30	10:20	N11
SwB	15:00–16:50	16:00	N16
SwA (SwC)	21:10–22:50	22:00	N22
Southern hemisphere			
SwB	03:10-05:00	04:00	S04
SwA (SwC)	09:10-11:00	10:00	S10
SwB	14:50–16:40	15:50	S16
SwA (SwC)	21:20–23:10	22:10	S22

* In the identifier, a letter and a digital symbol denotes the hemisphere and the central hour of MLT, respectively.

Ann. Geophys. Discuss., https://doi.org/10.5194/angeo-2019-40
Manuscript under review for journal Ann. Geophys.
Discussion started: 26 March 2019

Annales Geophysicae Discussions
Open Access
EGU

4 Data analysis

4.1 FAC densities

Statistically the large-scale R1 and R2 FAC densities are peaked at the dawn-dusk meridian. In this regard, satellites orbits on September 2017 are not optimal for identifying the R1/R2 extremes, since they are deviated from this meridian. However, the local time of satellite paths is representative enough to assess the evolution of these FACs. At dusk, the orbits of SwB are centered at about 16 MLT not far from the region, where the current density is expected to be maximal. On the night side, the orbits are centered at 04 MLT, where they overlay the ionospheric westward electrojet. SwA and SwC cross the pre-noon sector at about 10 MLT, where both the downward R1 and upward R2 are often identified. These satellites also cross the pre-midnight sector, where disturbances associated with substorms are expected. Aan example of the FACs measured along the SwB track is shown in **Fig. 3**. The 1-sec values are presented in **Fig. 3a**, while **Fig.3b** depicts the 21-point smoothed curve from which the dusk-side downward R1 and upward R2 currents can be clearly identified. In the near-pole region, FACs are almost absent. In the early morning a multi-layer structure is observed, in which the poleward currents are mostly positive, so they may be associated with downward the R1 FAC. The most equatorial currents are negative and thus represent the R2 FAC.

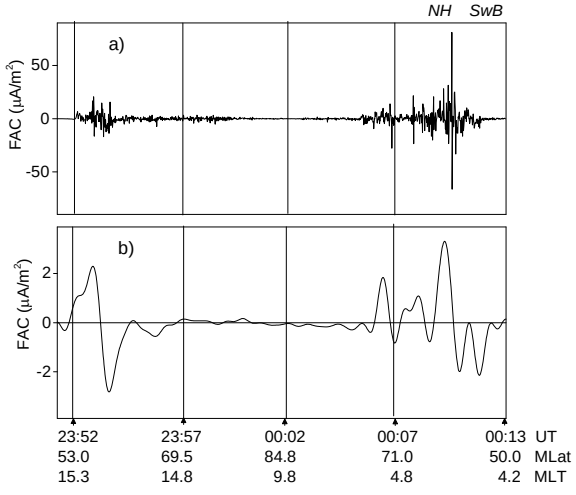

Figure 3: (a) 1-sec and **(b)** smoothed FACs measured by SwB in the northern polar region between 23:50 UT, 7 September, and 00:13 UT, 8 September.

Ann. Geophys. Discuss., https://doi.org/10.5194/angeo-2019-40
Manuscript under review for journal Ann. Geophys.
Discussion started: 26 March 2019

Annales Geophysicae Discussions
Open Access
EGU

To demonstrate the temporal evolution of FACs during the pre-storm and storm-time period, in **Fig. 4** the FAC intensities for each MLT sector is presented separately for the northern (**Fig. 4a–4d**) and southern (**Fig. 4e–4h**) hemispheres. Each red (blue) point is determined by averaging the positive (negative) FAC densities from a current-free location at the lowest and highest MLat of each crossing. These total densities correlate with the densities averaged over the track. In each plot of **Fig. 4**, the shading depicts the daily variation of MLT in such a way that a darker shade corresponds to a later MLT for a given range (cf. **Fig. 2b**). It can be seen that the measured FAC densities do not exhibit any systematic changes associated with the precession of the orbit.

FACs shown in **Fig. 4** exhibit three pronounced peaks: the first, smaller peak occurs on September 7, while the two higher peaks occur at the very beginning and in the middle of September 8. The intensity of a particular peak varies in different MLT sectors. Comparing **Fig. 1** and **Fig. 4** one can notice that the successive increases of FACs coincide with the perturbations in the SYM-H index. The first intensification of FAC (up to 1 $\mu A/m^2$) occurs at ~00 UT, Sept 7, when the SW dynamic pressure front impinges the magnetosphere causing a positive excursion of SYM-H. The dayside FACs (**Fig. 4a, b, e, f**) respond without any delay to this shock, while the nightside FACs (**Fig. 4c, d, g, h**) start to increase later, so that their peaks are rather associated with a moderate substorm seen in the AL index at ~8 UT, 7 September.

Ann. Geophys. Discuss., https://doi.org/10.5194/angeo-2019-40
Manuscript under review for journal Ann. Geophys.
Discussion started: 26 March 2019

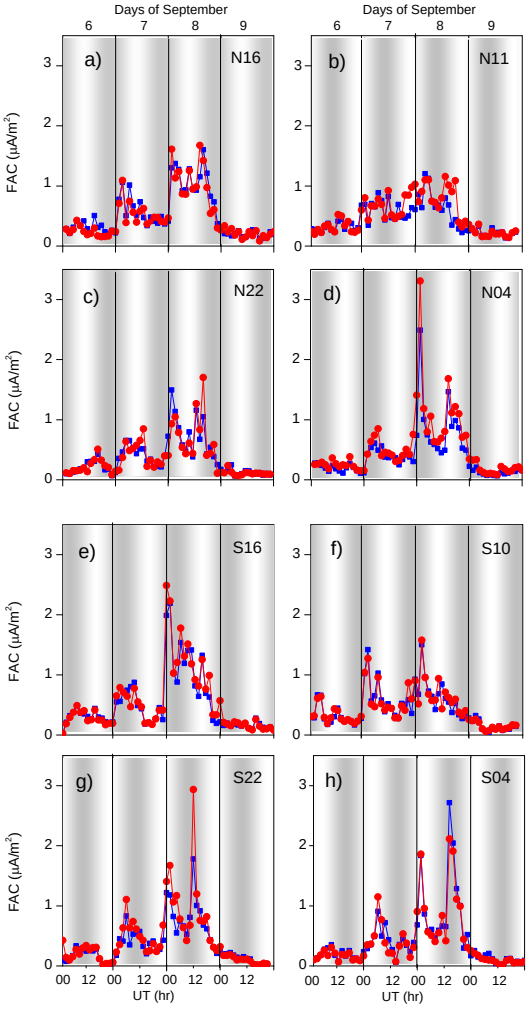

Figure 4: Average FAC densities in the four MLT sectors: **(a-d)** in the northern and **(e-h)** southern hemispheres, 6-9 September, 2017. The track identifier (see **Table 1**) is shown in the right upper corner of each plot. The downward and upward FAC is shown in red and blue, respectively. A darker shade corresponds to a later MLT for a given MLT range.

Ann. Geophys. Discuss., https://doi.org/10.5194/angeo-2019-40
Manuscript under review for journal Ann. Geophys.
Discussion started: 26 March 2019

Annales Geophysicae Discussions

A dramatic increase of FACs is caused by arrival of the second SW shock, which triggers the main phase of magnetic storm accompanied by a major substorm. After ~00 UT on Sept 8 the SYM-H and AL index drops to -150 and -2300 nT. During these perturbations FACs are intensified at all MLTs. The largest peak (up to 3.2 $\mu A/m^2$) is observed in the post-midnight sector in the northern hemisphere (**Fig. 4d**). The next increase in FACs occurs at ~12 UT on September 8 in association with the second major substorm (AL=-2000 nT) and the second drop of SYM-H down to -100 nT. The largest FACs (up to 3 $\mu A/m^2$) are observed in the night side in the southern hemisphere (**Fig. 4g, h**). In the day side, the response of FACs to the substorm intensification is weaker, although the current densities remain elevated throughout the day. All FACs fall to pre-storm levels by September 9.

Comparison of the evolution of FAC intensity with the SW and geomagnetic parameters during the period of 6-9 September reveals that the storm-time FACs are, on average, by several times larger than the quiet-time ones. The best coherence exists between FACs, especially in the night side, and substorm activity (AL index). Although FACs are considerably enhanced during a magnetic storm, the correlation between the current densities and SYM-H is relatively weak. Also there is no simple relation with any isolated SW input, such as the IMF or the SW dynamic pressure.

4.2 Dawn-dusk asymmetry

During the event of September 2017 a considerable dawn-dusk asymmetry in the storm-time FACs is revealed. Although the estimate is based on a limited number of crossings and does not allow calculating the total FAC, the current densities summed separately over the dawn and dusk sides may serve as a proxy. The sums of the upward/downward FAC densities for the four MLT sectors and for dawn and dusk sides are presented in **Table 2**. All parts of the tracks which fall into the 00-12 MLT (12-00 MLT) sector are considered to be related to the dawn (dusk) side.

For any given pass, the net summed FAC density is frequently nonzero. As seen in **Table 2 (**columns 3 and 4) the average net FACs summed over the entire 4-day interval in a particular MLT range, is also nonzero. The difference between summed upward and downward current densities varies from 1 to 15%. If the MLT sectors are combined in pairs in order to obtain the currents summed over the dawn and dusk, the prevalence of the dusk-side downward current is revealed. From the FAC values presented in columns 5 and 6 one can see that in both hemispheres the dusk-side downward current is stronger than all the other currents. This predominance implies an additional amplification of the storm-time R2 FAC on the dusk side, which is related to the partial ring current. Thus the estimation based on the summed FAC densities does indicate the existence of the storm-time dawn-dusk asymmetry.

Ann. Geophys. Discuss., https://doi.org/10.5194/angeo-2019-40
Manuscript under review for journal Ann. Geophys.
Discussion started: 26 March 2019

Annales Geophysicae Discussions

Table 2. Net summed upward (negative) and downward (positive) FAC densities for all passes on 6-9 September

Side	MLT range (as at 50° MLat)	Summed FAC densities (μA/m^2)			
		up	down	up	down
Northern Hemisphere					
dawn	9.5 – 11.5	-23.3	+23.4	-53.6	+53
	2.9 – 4.5	-31.3	+29.6		
dusk	21.1 – 22.7	-27	+30.1	-52.7	+60
	15.4 – 16.8	-24.7	+29.9		
Southern Hemisphere					
dawn	9.1 - 10.7	-26.8	+27.4	-50.5	+52.7
	3.3 – 4.7	-23.7	+25.3		
dusk	21.1 – 23.2	-23.8	+27.2	-52.5	+58.9
	15.0 – 16.5	-28.7	+31.7		

4.3 Dynamics of the equatorial boundary

It is well established that the enhanced SW input and the pile-up of open magnetic flux during a geomagnetic storm results in the equatorward expansions of the polar cap and the auroral oval as a whole (e.g. Milan et al., 2004). Following the magnetospheric dynamics FACs also move equatorward. **Fig. 5** shows the evolution of the equatorward boundary (EqB) of FACs on 6-9 September. The EqB is determined as the lowest latitude at which FACs are terminated. This latitude is determined using the 21-point sliding window applied to the 1-sec data according to the following criteria: at least eight values before and after the central point do not exceed 0.1 μA/m^2. Than the results are checked visually in order to avoid the erroneously calculated latitudes, that may happen, e.g., if a latitudinal gap between R1 and R2 occur. When calculating EqB, no separation between the up- and downward large-scale FACs has been made.

From **Fig. 5** one can see that during the pre-storm time FACs are observed mainly poleward of 60° MLat. During the storm main phase (8 September) FACs are shifted equatorward and EqB is found at 50° MLat. Unlike the current density, which exhibits sharp spike-like increases, temporal variations of EqB are relatively smooth. Comparing **Fig. 1** and **Fig. 4** one can see that EqB more closely follows the variation of SYM-H. Considerable equatorward shifts of EqB are associated with the modest substorms occurred before the storm main phase in the middle of 6 and 7 September. Upon arrival of the SW shock at the very end of September 7, EqB drops below 55° MLat, then tends to

Ann. Geophys. Discuss., https://doi.org/10.5194/angeo-2019-40
Manuscript under review for journal Ann. Geophys.
Discussion started: 26 March 2019

recover, and then drops again following the second intensification of the storm. Note that almost no difference in evolution in the day- and nightside EqBs is observed during the main and recovery phases.

Prior the storm main phase, in both hemispheres the prenoon EqB is found considerably poleward compared to the EqB location at other MLTs. The effect is well seen during the two time intervals: from ~22 UT, Sept 6 till 06 UT, Sept 7 and after 12 UT on September 7. Both intervals are dominated by the northward IMF (sf. **Fig. 1**), so that a shrinking of the polar cap and a poleward shift of the auroral oval is expected. With regard to the position of FACs, the displacement of its equatorward boundary is seen only in the pre-noon sector, while the other local times remain unaffected.

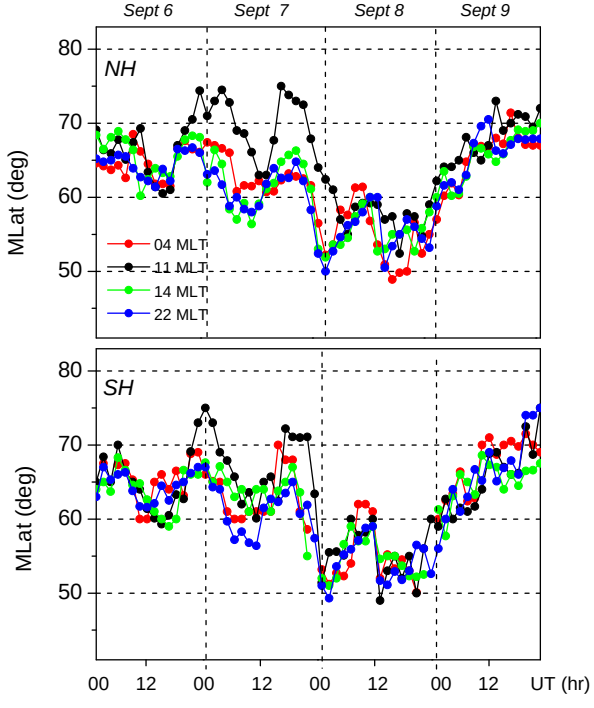

Figure 5: Magnetic latitude of the FAC equatorward boundaries in the northern (top) and southern (bottom) hemispheres for four MLT (see **Table 1**) sectors centered at approximately 04, 10, 16 and 22 MLT (see Table 1) on 6-9 September 2017.

Ann. Geophys. Discuss., https://doi.org/10.5194/angeo-2019-40
Manuscript under review for journal Ann. Geophys.
Discussion started: 26 March 2019

Annales Geophysicae Discussions
Open Access
EGU

4.4 Small-scale FACs

FACs appear on a wide range of scales from large-scale sheet-like currents of hundreds kilometers width to very small-scale filamentary currents of hundreds meters width. The current intensity vary inversely with scale so that large-scale currents are typically a few μA/m^2, whereas the smaller scale (down to 10 km) are a few tens μA/m^2. The standard *Swarm* time-series provide the resolved spatial scale of ~7.5 km. The quasi-instantaneous amplitudes of these small scale component of FACs are often much larger than the stationary R1/R2 FACs. To obtain the time-series of peak current densities, the largest positive and negative 1-sec values were selected from each crossing of a given MLT time sector irrespective of the hemisphere. The time-series of peak values are presented in **Fig. 6**. From the figure one can see that the small-scale peaks may be more than an order of magnitude larger than the FACs averaged over a track. During the disturbed period, starting with the compression of the magnetosphere on September 7, the amplitude of FACs tends to increase. Two intense substorms occurring during the storm main phase are accompanied by an additional strengthening of small-scale FACs. Both the up- and downward currents strengthen with increased geomagnetic activity and attain their extremes of ~80 μA/m^2) at the very beginning of 8 September. Note that some peaks may be missed due to a sparse spatial coverage.

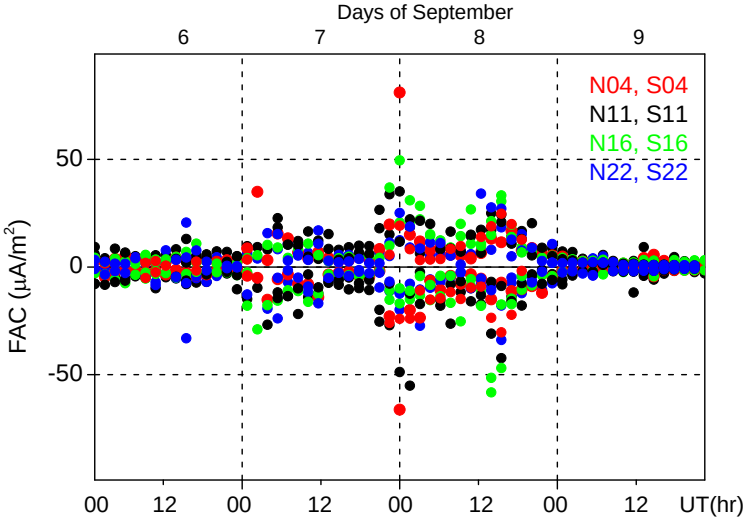

Ann. Geophys. Discuss., https://doi.org/10.5194/angeo-2019-40
Manuscript under review for journal Ann. Geophys.
Discussion started: 26 March 2019

Annales Geophysicae Discussions
Open Access
EGU

Figure 6: The largest positive and negative 1-sec current densities for four MLT sectors on 6-9 September.

In **Fig. 7**, the correlations between the magnetic latitudes, at which the small-scale FACs of opposite polarities are observed, are presented separately for the four MLT sectors in the northern hemisphere. In the pre-noon sector (**Fig. 7a**), the correlation coefficient between the latitudinal positions of the up- and downward FACs is 0.94. This is indicative of a large population of the paired, closely adjacent small-scale currents of opposite polarity (bipolar structures). In the post-noon/dusk sector (**Fig. 7b**) the correlation coefficient decreases down to 0.78. Slightly weaker correlation (cc=0.75) is observed in the pre-midnight sector (**Fig. 7c**). At the early morning hours (**Fig. 7d**) the correlation is poor (cc=0.53). Despite some spatiotemporal ambiguity inherent in single satellite observations, it can be speculated that at 03-05 MLT the up- and downward currents appear less frequently in pair but rather are separated by a distance greater than 8 km.

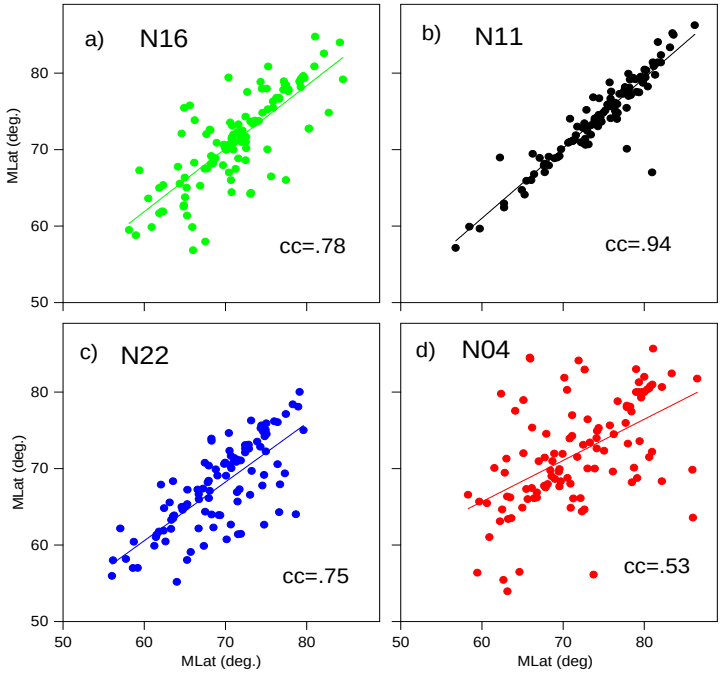

Ann. Geophys. Discuss., https://doi.org/10.5194/angeo-2019-40
Manuscript under review for journal Ann. Geophys.
Discussion started: 26 March 2019

Annales Geophysicae Discussions

Figure 7: Correlations between MLats, at which the up- and downward FACs are observed in the four MLT sectors: **(a)** post-noon/dusk, **(b)** pre-noon, **(c)** pre-midnight, **(d)** post-midnight.

4.5 Small-scale FACs of extreme amplitude

As seen in **Fig. 6**, a pair of the most intense upward and downward small-scale FACs is observed by SwB in the early morning MLTs. Just after the midnight of 7-8 September the SwB satellite traverses the latitudinal range of 60-80° MLat from north to south over the geographic area of the Barents Sea. The 1-sec FACs and plasma parameters (the electron density, Ne and temperature, Te, and the spacecraft electric potential, U_{sc}) measured by SwB for a period of 00:08:00-00:12:00 UT on 8 September during the growth phase of the first storm-time substorm are shown in **Fig. 8**. The original current densities are superimposed to the 21-point FFT smoothed curve, which reveals a multi-layer structure with several large-scale upward and downward FACs (**Fig. 8a**). Among them, the strongest (up to 30 $\mu A/m^2$) is the downward R1 FAC located at ~62° MLat. At 00:10:18 and 00:10:19 UT (latitudinally in between the downward R1 and upward R2 FACs) the satellite observes a pair of downward (81 $\mu A/m^2$) and upward (-66 $\mu A/m^2$) peaks. These paired small-scale up- and downward FACs of comparable values form a bipolar structure in which the currents are balanced and likely closed locally.

This current structure is accompanied by an increase in Ne. A narrow peak in Ne up to $77 \cdot 10^3$ cm^{-3} (**Fig. 8b**) and an increase of Te up to about 10^4 K on average (**Fig. 8c**), that is ~50% above their ambient values, are observed at 00:10:23 UT. Elevations of Te are observed in a wider region slightly poleward of the enhanced Ne. The plasma disturbances are clearly seen in U_{sc}, which is proportional to $-k \cdot Te$ (k is the Boltzmann constant). Note, the level of noise for the U_{sc} channel is much lower compared to that for the Te channel (0.4 and 2% for U_{sc} and Te, respectively). **Fig. 8d** shows a reduction of U_{sc} started at 00:09:56 UT and peaked at 00:10:08 (-12 V) and at 00:10:20 UT (-8 V), the average decrease is -5 V. The width of the region of the Te and U_{sc} perturbations is several times the width of the pair of extreme FACs and Ne. The localized increase of Ne and consequent conductance enhancement are likely due to precipitating electrons. The observed plasma and current perturbations are similar to those associated with auroral arcs (Opgenoorth et al. 1990; Lyons, 1992; Lewis et al., 1994; Johnson et al., 1998; Aikio et al., 1993). In particular, Aikio et al. (2002) studied the current system of arcs in the evening sector, where the background electric field is northward. It was shown that for arcs located within the northward convection electric field currents flow downward on the equatorward side of the arcs, then poleward, and upward from the arcs. The arcs are associated with an enhanced northward-directed electric field region on the equatorward side of the arc. An enhancement in the electric field starts already several tens km equatorward of the arc edge.

Ann. Geophys. Discuss., https://doi.org/10.5194/angeo-2019-40
Manuscript under review for journal Ann. Geophys.
Discussion started: 26 March 2019

Annales Geophysicae Discussions
Open Access
EGU

During the storm under consideration the bipolar FAC pattern observed at 00:10 UT is located in the morning sector, where the background electric field is expected to be southward. This is confirmed by the SuperDARN-based convection model (http://vt.superdarn.org/tiki-index.php?page=ASCIIData), which predicts in the region of the SwB observations the magnitude of the southward and westward component of about 6.5 mV/m and 0.5 mV/m, respectively. For morning side arcs an enhanced southward electric field on the poleward side of the arc is expected. In this case the current pattern consists of a downward FAC on the poleward side of the arc connected to an upward current above the arc by an equatorward ionospheric closure current. This is exactly what is seen in **Fig. 8a**: when SwB flies away the pole, it first observes a positive spike (downward FAC) and then a negative spike (upward FAC). Since the width of the region of enhanced Ne is ~30 km, the arc is relatively narrow. Comparing **Fig. 8a** and **Fig. 8b** one can see that the paired FACs is located at the poleward side of the region of enhanced Ne. Note, that in **Fig. 8b** a sharp increase in Ne up to ~80 $\cdot 10^3$ cm^{-3} is preceded by a weaker spike-like drop down to ~30 $\cdot 10^3$ cm^{-3}. A decrease in Ne (which is usually much less pronounced than a decrease due to precipitating electrons) is associated with a downward FAC observed at the opposite boundary of the arc. Elevations of Te are created by electric fields which can arise within narrow region adjacent to the northern side of the auroral arc (**Fig. 8c, d**).

Ann. Geophys. Discuss., https://doi.org/10.5194/angeo-2019-40
Manuscript under review for journal Ann. Geophys.
Discussion started: 26 March 2019

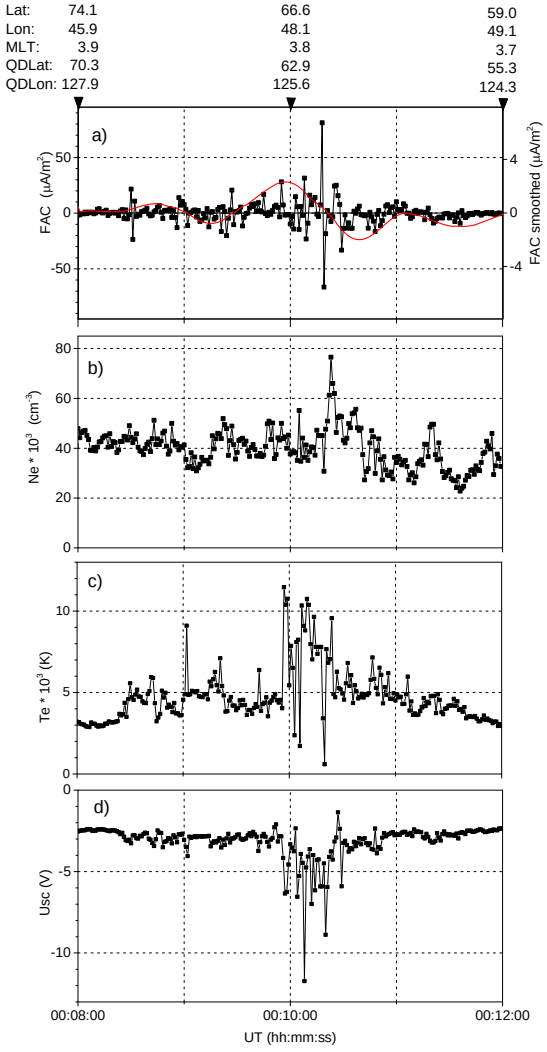

Figure 8: The 1-sec values of **(a)** FAC density, **(b)** Ne, **(c)** Te, and **(d)** Usc measured along the SwB track at 00:08:00 – 00:12:00 UT, 8 September. In the upper plot the 21-point smoothed FAC density is also shown. Geographic and geomagnetic coordinates are shown on the top.

Ann. Geophys. Discuss., https://doi.org/10.5194/angeo-2019-40
Manuscript under review for journal Ann. Geophys.
Discussion started: 26 March 2019

Annales Geophysicae Discussions
Open Access
EGU

5 Discussion

5.1 Small-scale FACs

Due to their large amplitudes medium and small-scale FACs play an important role for the energy input to the upper atmosphere. In several previous studies, the FACs associated with arcs were estimated as 1-10 μA/m^2 (Bythrow and Potemra, 1987; Elphic et al., 1998; Janhunen et al., 2000). Larger range of current densities, varying between 4 and >40 μA/m^2, has been observed (Aikio et al., 2002) and even more intense small-scale FACs, up to hundred of μA/m^2, at the edges of arcs have been measured (Marklund et al. 1982; Bythrow et al. 1984). Such a large range of the FACs estimates is likely related to its different scales, because for arcs with very sharp electron density gradients, the FACs associated with ionospheric currents flow in narrow regions at arc edges. If the real widths are smaller, the current densities will be larger.

During the September 2017 magnetic storm one of the *Swarm* satellites managed to observe a pair of the most intense small-scale FACs of opposite polarity, the magnitude of which are approximately +80 and -70 μA/m^2. These up- and downward FACs are separated in a fraction of degree in MLat. The FACs occur just prior of the substorm onset and they located in the region between R1 and R2 in the vicinity of the newly developed ionospheric WEJ. The polarity reversal captured by the *Swarm* data for two consecutive seconds implies a quite localized current closure through the ionosphere mostly via Pedersen horizontal currents. Although without optical data one could not make a strict conclusion, the small-scale bipolar FAC pattern accompanied by a localized enhancements in Ne and Te are likely associated with mesoscale discrete aurora. One-to-one correspondence of small-scale FACs with localized electron precipitation events has been previously observed (Fukunishi et. al., 1991).

The considerably elevated Te within the arc and just poleward of the arc is associated with a local amplification of electric field. The SwB observations are in agreement with the disturbances expected for the acrs occurred in the morning side, where the ambient electric field is southward. The observed features are resemble to those reported by Aikio et al. (2002) but bearing in mind that the latter are related to the evening sector, where the background electric field is northward.

Based on *Swarm*/*THEMIS* ASI observations Wu et al. (2017) has associated multiple auroral arcs with up/down current pairs. For these arcs unipolar and multipolar FAC systems with current densities of about a few μA/m^2 have been observed. Arcs in unipolar FAC systems have a typical width of 10–20 km and a spacing of 25–50 km. Arcs in

Ann. Geophys. Discuss., https://doi.org/10.5194/angeo-2019-40
Manuscript under review for journal Ann. Geophys.
Discussion started: 26 March 2019

Annales Geophysicae Discussions
Open Access
EGU

multipolar systems are wider and more separated. In the bipolar structure observed by SwB during the September 8 event, the current density exceeds the density observed by Wu et al. (2017) at least by a factor of ten, while the spatial extend of FACs is smaller. This difference implies the existence of sharp electron density gradients at arc edges.

Filamentary high-density structures are always presented in the *Swarm* observations. This confirms the fact that a substantial fraction of R1/R2 currents is composed of many small-scale FACs. The narrow high-density currents are averaged out when integrated over a FAC region, so that multilayer structures of steady large-scale FACs depicted by Iijima and Potemra (1978) can be revealed after a proper smoothing. From a statistical study of the temporal and spatial-scale characteristics of different FAC types derived with the *Swarm* satellites Luhr et al. (2015) have shown that small-scale, up to some 10 km FACs are carried predominantly by kinetic Alfven waves. A persistent period of small-scale FACs of order 10 s, while large-scale FACs can be regarded stationary for more than 1 min. Neubert and Christiansen (2003) studied the morphology of very small-scale FACs from a survey of *Oersted* satellite 25 Hz data. These FACs are distributed in a broad region around the pre-noon and cusp region, and in the pre-midnight sector. It was found that at the considered time scale, instantaneous currents may reach the largest values up to 1000 $\mu A/m^2$, while the average current densities reach a maximum of 10 $\mu A/m^2$. McGranaghan et al. (2017) demonstrated a local time dependence in the relationships between large and small FAC scales (10–150 km width, density is up to 0.5 $\mu A/m^2$). It was found that linear relationships exist near dawn and dusk local times, while at noon and midnight local times no similar regularity is seen. The results are based at all available data from the *Swarm* satellites and the Advanced Magnetosphere and Planetary Electrodynamics Response Experiment (AMPERE) irrespective of the level of geomagnetic activity.

During the disturbed period on September 2017, the amplitudes of quasi-instantaneous FACs are often considerably larger than the average values. Although the amount of data is not sufficient for a rigorous conclusion, a preliminary analysis (not presented here) shows that in all MLT sectors the statistical relationship between average and quasi-instantaneous peak densities is linear. A tendency of higher correlations (up to cc=0.8) is found at dawn and dusk, while poorer correlations are in the pre-noon sector.

5.2 Large-scale FACs

Evolution of large-scale FACs during the September 2017 storm is in general agreement with regularities observed previously by Wang et al. (2004) during the intense 2003 geomagnetic storms. The common feature of all storm-times is the equatorward motion of FACs correlating with the storm intensity. At the same time, some notable features are found for the September 2017 storm. One of them is a large equatorward expansion of FACs. For the 2003 storms, the minimum latitude of the equatorial boundaries (EqB) of FACs are limited to 52-56° MLat (Wang et al., 2004), while

Ann. Geophys. Discuss., https://doi.org/10.5194/angeo-2019-40
Manuscript under review for journal Ann. Geophys.
Discussion started: 26 March 2019

for the 2017 storm the boundaries expand as low as 50° MLat. Below this latitude, saturation occurs. The latitudinal positions of EqB generally follow the Dst (SYM-H) index variation. However, despite the 2017 storm is considerably weaker (Dst≈-100 nT) than the 2003 storms (Dst≈-400 nT), in the 2017 event, the FACs are expanded to lower latitudes.

Linear dependence between latitudinal boundaries of the FAC sheets upon the dayside merging electric field, the AE and Dst indices has been reported by Xiong et al. (2014). It was pointed out that toward high activity a saturation of equatorwards expansion seems to set in. In 2017, the FAC boundaries primarily respond to the storm development, which is mainly governed by the IMF Bz turning southward. Also, FACs are shifted further equatorward during the storm-time substorms. Even a relatively minor substorm occurred prior the storm causes an equatorward displacement of FACs. The lowest latitude of EqB is observed when the SYM-H and AL indices reach their minimums. During the storm main phase no considerable difference between the latitudinal positions of EqB in different MLT sectors is observed. After ~12 UT on September 9, the day- and nightside EqBs recover to undisturbed position (about 70° MLat), although the storm recovery phase continues (SYM-H ≈ -50 nT). Previous analysis of the latitudinal shift of the polar cap boundaries based on the *Image* observations during a magnetic storm has shown that, if the IMF Bz turns northward, the dayside boundary recovers much faster than the nightside boundary (Lukianova and Kozlovsky, 2013). In the *Swarm* data the poleward boundaries of the FAC region are not clearly identified. However, it seems that the nightside EqB recovery does not exhibit any delay compared to the dayside EqB. Prior the storm main phase, when the IMF Bz is northward, the pre-noon EqB is located at higher latitudes (~75° MLat) compared to the other MLT sectors (~65 MLat).

Determination of the poleward FAC boundary is less reliable than determination of the equatorial one. It is because in some cases (if the satellite does not traverse the central polar cap) the FACs are observed during the entire crossing of the polar region, so it is not possible to construct a continuous time series of the polar latitudes at which FACs are terminated. Examination of the available incomplete time series (not shown) reveals that prior the storm the poleward boundary of the FAC region tends to follows the evolution of the polar cap boundary, which depends on storm intensity (Milan et al., 2010) and orientation of the IMF vector (Lukianova and Kozlovsky, 2011).

Evolution of FAC densities generally follows the same tendencies as the latitudinal position of EqB. During the pre-storm and disturbed periods, FACs are intensified in accordance with the auroral magnetic activity. However, the latitudinal displacement of FACs is more gradual and smooth compared to the changes in current intensity. The FAC densities, especially in the night side, promptly respond to the onset of storm-time substorms. The fact that the R1/R2 current intensity is controlled most efficiently by substorm evolution was pointed out by He et al. (2014). On

Ann. Geophys. Discuss., https://doi.org/10.5194/angeo-2019-40
Manuscript under review for journal Ann. Geophys.
Discussion started: 26 March 2019

September 8, just upon the shock arrival, the dayside FACs increase (almost without delay) in response to the increased SW dynamic pressure. The largest current density averaged over a pass is observed at the early morning and pre-midnight local times during the peak of substorm expansion on September 8. At the end of the next day, September 9, FACs return to an undisturbed level of <0.1 $\mu A/m^2$. This level corresponds to the statistical FAC densities for the zero IMF (Papitashvili et al., 2002). Comparing the evolution of the FAC densities and the equatorial boundary positions during the storm recovery, one can see that the densities decay much faster than the boundaries return to their quiet time positions.

The *Swarm* observations provide some indications of the dawn-dusk asymmetry in the FAC distribution. While the summed FAC intensities are comparable between the two hemispheres, the positive and negative densities in a certain MLT sector are slightly imbalanced and the net current is nonzero. The dawn-dusk asymmetry is revealed by comparing the up- and downward FACs, which are summed separately over dusk and dawn. The largest values are characteristics of the dusk-side downward R2 FACs. The observed imbalance in FACs is likely related to an intensification of partial ring current (PRC), which is connected to R2 FAC. Strengthening of PRC may also lead to asymmetric dusk-side inflation of the geomagnetic field lines. The asymmetry in the equatorward displacement of R1 and R2 at the peak of the major storm on August, 2000, has been reported by Anderson and Korth (2007). For the storm of September 2017 almost no difference in the equatorward shift of the dusk and dawn side FACs is observed. During this particular storm the dawn–dusk asymmetry is rather manifested in the enhanced density of R2 FAC on the dusk side.

6 Conclusion

Characteristics of FACs inferred from the *Swarm* observations during the severe magnetic storm of 6-9 September 2017 are presented. This storm is the two-step one and the intense substorms occur in the course of the storm main phase. The satellites cross the pre-midnight, pre-noon, pre-dusk and pre-midnight sectors. The following features of the storm-time FACs are found.

Evolution of the current intensities and the latitudinal position of the equatorward boundaries of the FAC region are controlled by a storm-substorm interplay. The night-time FAC densities primarily follow the substorm development. At the peak of substorm, the FAC densities averaged over a track within a given MLT sector, reach 3 $\mu A/m^2$, while the undisturbed level is about 0.2 $\mu A/m^2$. The dawn–dusk asymmetry is manifested in the enhanced dusk side (downward) R2 FAC in both hemispheres.

The equatorward displacement of FAC sheets (in the north and south and at all MLTs) correlates with the storm intensity as monitored by the SYM-H index. The minimum latitude of the equatorial FAC boundaries is limited to 50° MLat, below which saturation occurs. Displacement of FAC sheets is more gradual and occurs with a considerable time delay compared to the changes in current intensity.

The R1/R2 currents are composed of many small-scale filamentary structures of high-density FACs, which are always presented in the *Swarm* observations. A bipolar structure of FACs (up to ~80 μA/m^2, 7.5 km width) of opposite polarities is observed in the vicinity of the newly developed WEJ just prior of the substorm onset. Simultaneous plasma perturbations indicate that the bipolar FAC pattern is associated with mesoscale auroral arc.

Data availability: The data used for the publication of this research are freely available from the *Swarm* Science Team web site (ftp://swarm-diss.eo.esa.int). Data selected for the analysis are available upon request (RL).

Competing interests: The author declare that she has no conflict of interest concerning this paper.

Acknowledgement

Swarm data are available through the European Space Agency Online platform (ftp://swarm-diss.eo.esa.int), after registration. We acknowledge the *Swarm* Science Team for providing the level 2 data and the *Swarm* visualization tool (https://vires.services/). The OMNI data on the solar wind, interplanetary magnetic field and geomagnetic indices are obtained from NASA/GSFC's Space Physics Data Facility's CDAweb service (http://omniweb.gsfc.nasa.gov/). This research was partly supported by the RFBR (grant 17-05-00475).

References

Aikio, A.T., Opgenoorth, H.J., Persson, M.A.L., and Kaila, K.U.: Groundbased measurements of an arc-associated electric field, J. Atmos. Terr. Phys., 55, 797–808, 1993.

Aikio, A.T., T. Lakkala, A. Kozlovsky, and Williams, P.J.S.: Electric fields and currents of stable drifting auroral arcs in the evening sector, J. Geophys. Res., 107(A12), 1424, doi:10.1029/2001JA009172, 2002.

Akasofu, S.-I.: The development of the auroral substorm, Planet. Space Sci., 12, 273–282, 1964.

Anderson, B.J., and Korth, H.: Saturation of global field aligned currents observed during storms by the Iridium satellite constellation, J. Atmos. Solar-Terr. Phys., 69, 166–169, 2007.

Bythrow, P.F., and Potemra, T.A.: Birkeland currents and energetic particles associated with optical auroral signatures of a westward traveling surge, J. Geophys. Res., 92, 8691–8699, 1987.

Chertok, I.M., Belov, A.V., and Abunin, A.A.: Solar eruptions, Forbush decreases, and geomagnetic disturbances from outstanding active region 12673, Space Weather, 16, 1549–1560, doi:10.1029/2018SW001899, 2018.

Clilverd, M.A., Rodger, C.J., Brundell, J.B., Dalzell, M., Martin, I., Mac Manus, D.H., et al.: Long-lasting geomagnetically induced currents and harmonic distortion observed in New Zealand during the 7–8 September 2017 disturbed period, Space Weather, 16, 704-717, doi:10.1029/2018SW001822, 2018.

Curto, J.J., Marsal, S., Blanch, E., and Altadill, D.: Analysis of the solar flare effects of 6 September 2017 in the ionosphere and in the Earth's magnetic field using spherical elementary current systems, Space Weather, 16, doi:10.1029/2018SW001927, 2018.

Dunlop, M. W., Yang, Y.-Y., Yang J.-Y., Lühr, H., Shen, C., et al.: Multispacecraft current estimates at swarm, J. Geophys. Res. Space Phys., 120, doi:10.1002/2015JA021707. 2015.

Elphic, R.C., Bonnell, J.W., Strangeway, R.J., Kepko, L., Ergun, R.E., et al.: The auroral current circuit and field-aligned currents observed by FAST, Geophys. Res. Lett., 25, 2033– 2036, 1998.

Iijima, T., and Potemra T.A.: The amplitude distribution of field-aligned currents at northern high latitudes observed by Triad, J. Geophys. Res., 81(13), 2165–2174, doi:10.1029/JA081i013p02165, 1976.

Iijima, T., and Potemra, T.: The amplitude distribution of field-aligned currents associated with substorms, J. Geophys. Res., 83, 599–615, 1978.

Janhunen, P., Olsson, A., Amm, O., and Kauristie, K.: Characteristics of a stable arc based on FAST and MIRACLE observations, Ann. Geophys., 18, 152– 160, 2000.

Johnson, M.L., Murphree, J.S., Marklund, G.T., and Karlsson, T.: Progress on relating optical auroral forms and electric field patterns, J. Geophys. Res., 103, 4271–4284, doi:10.1029/ 97JA00854, 1998.

Juusola, L., Kauristie, K., Vanhamaki, H., Aikio, A., and van de Kamp M.: Comparison of auroral ionospheric and field-aligned currents derived from Swarm and ground magnetic field measurements, J. Geophys. Res. Space Phys., 121, 9256–9283, doi:10.1002/2016JA022961, 2016.

Fukunishi, H., Fujii, R., Kokubun, S., Tohyama, F., Mukai T., and Oya H.: Small-scale field-aligned currents observed by the Akebono (EXOS-D) satellite, Geophys. Res. Lett., doi:10.1029/91GL00036, 1991.

He, M., Vogt, J. Lühr, H., and Sorbalo, E.: Local time resolved dynamics of field-aligned currents and their response to solar wind variability, J. Geophys. Res. Space Phys., 119, 5305–5315, doi:10.1002/2014JA019776, 2014.

Green, D.L., Waters, C.L., Anderson, B.J., and Korth, H.: Seasonal and interplanetary magnetic field dependence of the field-aligned currents for both Northern and Southern Hemispheres, Ann. Geophys., 27, 1701–1715, www.ann-geophys.net/27/1701/2009/, 2009.

Lewis, R.V., Williams, P.J.S., Jones, G.O., Opgenoorth, H.J., and Persson, M.A.L.: The electrodynamics of a drifting auroral arc, Ann. Geophys., 12, 478, 1994.

Lui, A.T.Y.: Current disruption in the Earth's magnetosphere: Observations and models, J. Geophys. Res., 101, 13 067–13 088, 1996.

Luhr, H., Park, J., Gjerloev, J.W., Rauberg, J., Michaelis, I., Merayo, J.M.G., and Brauer, P.: Field-aligned currents' scale analysis performed with the Swarm constellation. Geophys. Res. Lett., 42, 1–8, doi:10.1002/2014GL062453, 2015.

Lukianova, R., and Kozlovsky, A.: IMF B_y effects in the plasma flow at the polar cap boundary, Ann. Geophys., 29, 1305-1315, doi:10.5194/angeo-29-1305-2011, 2011.

Lukianova, R., and Kozlovsky, A.: Dynamics of polar boundary of the auroral oval derived from the IMAGE satellite data, Cosmic Res., 51(1), 46–53, 2013.

Lyons, L.R.: Formation of auroral arcs via magnetosphere-ionosphere coupling., Rev. Geophys., 30, 93–112, 1992.

Marklund, G., Sandahl, I., and Opgenoorth, H.: A study of the dynamics of a discrete auroral arc, Planet. Space Sci., 30, 179–197, doi:10.1016/0032-0633(82)90088-5, 1982.

McGranaghan, R.M., Mannucci, A.J., and Forsyth, C.: A comprehensive analysis of multiscale field-aligned currents: Characteristics, controlling parameters, and relationships, J. Geophys. Res.: Space Phys., 122, 11931–11960, doi:10.1002/2017JA024742, 2017.

Milan, S.E., Evans, T.A., and Hubert, B.: Average auroral configuration parameterized by geomagnetic activity and solar wind conditions, Ann. Geophys., 28, 1003–1012, www.ann-geophys.net/28/1003/2010/, 2010.

Milan, S.E., Cowley, W.H., Lester, M., Wright, D.M., Slavin, J.A., Fillingim, M., Carlson, C. W., and Singer, H.J.: Response of the magnetotail to changes in the open flux content of the magnetosphere, J. Geophys. Res., 109, doi:10.1029/2003JA010350, 2004.

Neubert, T., and Christiansen, F.: Small-scale, field-aligned currents at the top-side ionosphere, Geophys. Res. Lett., 30(19), 2010, doi:10.1029/2003GL017808, 2003.

Opgenoorth, H.J., Haggstrom, I., Williams, P.J.S., and Jones, G.O.L.: Regions of strongly enhanced perpendicular electric fields adjacent to auroral arcs, J. Atmos. Terr. Phys., 52, 449– 458, doi:10.1016/0021-9169(90)90044-N, 1990.

Papitashvili, V.O., Christiansen, F., and Neubert, T.: A new model of field-aligned currents derived from high-precision satellite magnetic field data, Geophys. Res. Lett., 29(14), 1683, doi:10.1029/2001GL014207, 2002.

Ritter; P., Lühr, H.: Curl-B technique applied to Swarm constellation for determining field-aligned currents, Earth Planets Space, 58(4), 463-476, 2006.

Swarm Level 2 Processing System Consortium. Detailed Processing Model (DPM) FAC (Tech. Rep. SW-DS-GFZ-GS-0002): Swarm Level 2 Processing System, 2012.

Tanskanen, E.I.: A comprehensive high-throughput analysis of substorms observed by IMAGE magnetometer network: Years 1993-2003 examined, J. Geophys. Res., 114, A05204, doi:10.1029/2008JA013682, 2009.

Wang, H., Luhr, H., Ma, S.Y., Weygand, J., Skoug, R.M., and Yin, F.: Field-aligned currents observed by CHAMP during the intense 2003 geomagnetic storm events, Ann. Geophys., 24, 311–324, SRef-ID:1432-0576/ag/2006-24-311, 2006.

Weimer, D.R.: Maps of ionospheric field-aligned currents as a function of the interplanetary magnetic field derived from Dynamics Explorer 2 data, J. Geophys. Res., 106, 2889-12902, 2001.

Wu, J., Knudsen, D.J., Gillies, D.M., Donovan, E.F., and Burchill, J.K.: Swarm Observation of Field-Aligned Currents Associated With Multiple Auroral Arc Systems, J. Geophys. Res.: Space Phys., 122, 10145–10156, doi:10.1002/2017JA024439, 2017.

Yasyukevich, Yu., Astafyeva, E., Padokhin, A., Ivanova, V., Syrovatskii, S., and Podlesnyi A.: The 6 September 2017 X-class solar flares and their impacts on the ionosphere, GNSS and HF radio wave propagation, Space Weather, 16, doi:10.1029/2018SW001932, 2018.